$Si_{0.7}Ge_{0.3}/Si$ Heterojunction Internal Photoemission Infrared Detector

T. L. Lin, J. S. Park, S. Gunapala, E. W. Jones, and H. M. Del Castillo

Center for Space Microelectronics Technology
Jet Propulsion Laboratory, California Institute of Technology
Pasadena, CA 91109

ABSTRACT

Single-layer and multi-layer $Si_{0.7}Ge_{0.3}/Si$ HIP detectors with cutoff wavelengths out to ~23 μm have been demonstrated. Near-ideal thermionic emission dark current characteristics and photoresponse at wavelength up to 20 μm were measured. The cutoff wavelength, λ_c, and the emission coefficient, C_1, of the HIP detectors were determined by the modified Fowler plot at the wavelength regime where the corresponding photon energies were smaller than the Fermi energy (-0.1 5 eV) of the degenerate $Si_{0.7}Ge_{0.3}$ layers. Similar optical and thermal potential barriers were obtained. The use of multiple $Si_{0.7}Ge_{0.3}/Si$ layers in the stacked HIP detector structure resulted in a significantly increased emission coefficient C_1 compared to the single-layer HIP detectors due to an enhanced internal photoemission efficiency without the loss of IR absorption.

1. INTRODUCTION

Silicon-compatible detectors are among the most promising infrared sensors for large focal plane array applications due to their advantages of uniformity, reliability, and easy integration with low-noise Si readout circuitry. The PtSi/p-Si Schottky photodiode is the most advanced Si-compatible IR detector, and state-of-the-art 640 x 480 and 1024 x 1024 element PtSi imaging arrays have been demonstrated for imaging in the 3-5 μm medium wavelength infrared (MWIR) region[1 -4]. The applications of the PtSi detector have been limited to the 1-3 and 3-5 μm spectral bands due to the fixed PtSi cutoff wavelength of ~5.7 μm. An extended cutoff wavelength will improve the cold night thermal imaging performance of focal plane arrays, although a lower operating temperature will be required to reduce the dark current. Previously, extension of the photoresponse into the long wavelength infrared (LWIR) spectral band, ranging from 8 to 14 μm, has been demonstrated for IrSi detectors [5,6]. However, the uniformity of IrSi arrays is substantially inferior to that of PtSi, possibly due to poor IrSi process repeatability. Formation of iridium silicate during the IrSi process has been reported previously [7]. Recently, by incorporating a p+ doping spike (1 nm thick) at the PtSi/Si interface, we have successfully demonstrated tailorable cutoff wavelengths for PtSi detectors ranging from 14 to 22 μm for the first time [8]. The tailorable cutoff wavelength of the doping-spike PtSi detector allows flexibility of optimizing the trade-off between responsive wavelength region and imaging system cooling requirements.

The photoresponse of the silicide IR detectors, such as the PtSi detector and the IrSi detector, can be characterized by the modified Fowler equation[9],

$$\eta = C_1 \frac{(h\nu - \Psi_0)^2}{h\nu} \qquad (1)$$

where C_1 is the Fowler emission coefficient, $h\nu$ is the photon energy, and Ψ_0 is the optical potential barrier determined by the spectral response. The detector dark current is dominated by the thermionic emission current, given by the Richardson equation

$$J_0 = A^{**} T^2 \exp(-\Psi_t / kT) \qquad (2)$$

where A^{**} is the Richardson constant, T is the absolute temperature, k is Boltzmann constant, and Ψ_t is the thermal potential barrier which can be determined by the Richardson plot. For the PtSi Schottky detector, the optical barrier potential Ψ_0 is usually 0.02 to 0.05 meV larger than the thermal potential barrier Ψ_t [1 O]. The discrepancy between Ψ_0 and Ψ_t results mainly from the energy loss of photo-excited

3

carriers by inelastic scattering prior to the carrier emission. Thus, to compensate for the energy loss, larger photon energy is required, resulting in a higher optical barrier Ψ_O. Consequently, a lower operating temperature is required for the PtSi detector to reduce the dark current compared to other detectors which do not have the potential discrepancy. In addition, the cooling penalty gets worse as the cutoff wavelength increases.

Previously, we have demonstrated an alternative Si-compatible LWIR detector, the $Si_{1-x}Ge_x/Si$ heterojunction internal photoemission (HIP) infrared detector, and tailorable cutoff wavelengths beyond 23 μm have been reported [10,1 1], and uncompensated thermal imagery in the 7.5 to 9.3 μm wavelength regime using a 400 x 400-element $Si_{1-x}Ge_x/Si$ HIP CCD array has been reported by Tsaur et. al. [1 2]. Furthermore, it has been observed that for the Si_xGe_{1-x}/Si HIP detector, the discrepancy between 'P_o and Ψ_t is negligible compared to the discrepancies of 20-50 meV usually observed for PtSi Schottky detectors [11].

This detector concept was first proposed by Shepherd, Vickers, and Yang in 1971 [13], Figure 1 shows the schematic device structure and the energy band diagram of the $Si_{1-x}Ge_x/Si$ HIP detector. It consists of a thin, degenerately doped p^+-$Si_{1-x}Ge_x$ layer as the emitter and a p-type Si substrate as the collector. The $Si_{1-x}Ge_x/Si$ valence band offset, which can be tailored by varying the Ge composition of the $Si_{1-x}Ge_x$ layer, was utilized as the potential barrier for the internal photoemission of photo-excited hole, providing a tailorable cutoff wavelength. The detection mechanism is similar to that of the PtSi Schottky detector, involving free-carrier absorption in the degenerately-doped $Si_{1-x}Ge_x$ layer followed by internal photoemission of the photo-excited holes over the $Si_{1-x}Ge_x/Si$ heterojunction barrier into the Si substrate.

In this paper, we report the performance of both single-layer and multi-layer $Si_{0.7}Ge_{0.3}/Si$ HIP detectors which exhibit photoresponse at wavelengths ranging from 2 to 20 μm. Cutoff wavelengths out to 23 μm have been determined by the modified Fowler plots at wavelengths near the cutoff. Furthermore, the optimization of the HIP detector structure was discussed using the emission coefficient C_1 as a figure-of-merit.

2. DETECTOR FABRICATION

The HIP detectors were fabricated by growing hetero-epitaxial $Si_{0.7}Ge_{0.3}$ layers on a double-side polished Si (100) wafer. The device structure incorporates p^+-substrate contacts and n-type guard rings which define the periphery of the active device areas to suppress edge leakage. Two HIP detector structures with single 10- and 30-nm-thick $Si_{0.7}Ge_{0.3}$ layers and one stacked HIP detector structure with two 5-

4

rim-thick p^+-$Si_{0.7}Ge_{0.3}$/30 -rim-thick i-Si multilayers were fabricated. The details of device fabrication can be found elsewhere [10,14].

3. DETECTOR CHARACTERISTICS

The infrared absorption of the $Si_{0.7}Ge_{0.3}$ layers were characterized by Fourier transform infrared spectrometer and is shown in Fig. 2 in terms of absorptance. The infrared absorption at wavelengths less than 3 μm was attributed to the intraband transition. For wavelength larger than 3 μm, the absorption was mainly due to the strong free-carrier absorption caused by the degenerate doping in the $Si_{0.7}Ge_{0.3}$ layers[13]. The infrared absorption of the 10- and 30-nm-thick $Si_{0.7}Ge_{0.3}$ layers increases with increasing wavelength and saturates to ~27% and 45% for wavelengths > 15 pm, respectively. The IR absorption of the two 5-rim-thick p^+-$Si_{0.7}Ge_{0.3}$/30-nm-thick i-Si multilayers for the stacked HIP detector is similar to that of the 10-rim-thick $Si_{0.7}Ge_{0.3}$ layer.

The current-voltage (I-V) characteristics of the HIP detectors were measured at temperatures ranging from 25 to 50 K. The dark current of the $Si_{0.7}Ge_{0.3}$/Si HIP detector was dominated by thermionic emission. Figure 3 shows the plot of J_o/T^2 vs $1/kT$ of a typical HIP detector with a 10-rim-thick $Si_{0.7}Ge_{0.3}$ layer at -0.5 V bias. Similar thermal potential barriers Ψ_t of 0.05, 0.058, and 0.053 eV were determined from the slopes of the linear portion of the plots for the two $Si_{0.7}Ge_{0.3}$/Si HIP detectors with 10- and 30-nm-thick $Si_{0.7}Ge_{0.3}$ layers and the stacked HIP detector, respectively. The effective heterojunction barriers Ψ_t are significantly lower than the expected valence band offset AE_v(~0.2 eV) between Si and $Si_{0.7}Ge_{0.3}$ due to the degenerate doping concentration (5 x 10^{20} cm-3) of the $Si_{0.7}Ge_{0.3}$ layers which moves the Fermi level below the valence band edge, i.e.,

$$\Psi_t = \Delta E_V - EF. \qquad (3)$$

From Eq. (3), the Fermi energy E_F in these degenerately doped $Si_{0.7}Ge_{0.3}$ layers is estimated to be ~ 0.15 eV. The Richardson constants A** determined from the ordinate intercepts at $1/kT = O$ were 4.4, 15.5, and 30.0 $A/cm^2/K^2$ for the two $Si_{0.7}Ge_{0.3}$/Si HIP detectors with 10- and 30-nm-thick $Si_{0.7}Ge_{0.3}$ layers and the stacked HIP detector, respectively.

Figure 4 shows the external quantum efficiency η at wavelengths ranging from 2 to 20 μm for the HIP detectors and the stacked detector. The detectors were cooled to 30K and biased at -0.5 V. These spectral responses were measured with front-side illumination using a 940K blackbody source. Neither an optical cavity nor an anti-reflection coating was incorporated in the HIP and the stacked HIP detectors. The QE increases initially with increasing wavelength to a maximum of ~ 8 % at 4-5 μm, and

then decreases because of the decreasing internal photoemission probability over the heterojunction barrier as the energy of the photo-excited carriers decreases. The initial increase of the QE results from the increase in free-carrier absorption, as shown in Fig. 2.

For the $Si_{0.7}Ge_{0.3}$/Si HIP detectors, the external QE is shown to increase with decreasing $Si_{0.7}Ge_{0.3}$ thickness. For example, the QE of the 10-rim-thick $Si_{0.7}Ge_{0.3}$/Si HIP detector at 12 μm is 0.94%, compared to 0.33% for the 30-nm-thick $Si_{0.7}Ge_{0.3}$/Si HIP detector. The optimal $Si_{0.7}Ge_{0.3}$ thickness is determined by the trade-off between the absorptance, A, which increases with an increasing thickness, and the internal photoemission efficiency, η_i, which increases with a decreasing thickness. Although the IR absorptance, A, for the 10-rim-thick $Si_{0.7}Ge_{0.3}$/Si HIP detector is - 60% that for the 30-nm-thick $Si_{0.7}Ge_{0.3}$/Si HIP detector (as shown in Fig. 2), the smaller thickness not only increases the elastic scattering of the photo-excited holes at the $Si_{0.7}Ge_{0.3}$/air interface and helps to redirect the holes toward the $Si_{0.7}Ge_{0.3}$/Si interface, but also reduces the inelastic hole-hole and hole-phonon scattering, resulting in a higher overall QE.

By incorporating multiple thin absorbing SiGe layers which are stacked between Si barriers, a higher internal photoemission efficiency can be achieved without any loss of IR absorption because each individual SiGe layer has a high η_i due to the small thickness and the absorption from each layer contributes to the total absorption. Furthermore, due to the applied electric field toward the Si substrate (z-direction), the photo-excited holes traveling opposite to z-direction will be redirected toward the Si substrate. This will further increase the internal quantum efficiency. As shown in Fig. 4, the stacked HIP detector shows broad photoresponse which extends to around 20 μm. The peak response lies at around 5 μm with 6 % external quantum efficiency. The response gradually decreases as the wavelength increases and a small bump is observed near 14 pm. The detector manifests about 4 % and 1.5940 QE at 10 μm and 15 μm wavelengths, respectively. The stacked SiGe/Si HIP detector exhibits a higher QE in the LWIR regime ($\lambda>10\mu m$) than the single-layer SiGe/Si HIP detectors. This can be due to the enhancement of internal photoemission efficiency η_i, especially in the long-wavelength regime where hot holes have small kinetic energies to cross over the potential barrier.

To evaluate the optimal detector structure for the $Si_{0.7}Ge_{0.3}$/Si HIP detector, a theoretical response model, similar to the modified Fowler plot, has been previously proposed to provide a figure-of-merit for comparison [1 4]. The model predicts the photoresponse of the HIP detector at wavelengths corresponding to photon energies less than the Fermi energy, corresponding to wavelengths close to the cut-off. It is important to model the detector response close to the cutoff wavelength, since a fast

6

response increase as the wavelength decreases from the cutoff will allow the detector to have useful sensitivity near the cutoff, thereby minimizing the extension of the cutoff wavelength and associated cooling requirements. The model is given by [14] :

$$\eta = \frac{A}{8\,E_F{}^{0.5}\,(E_F\,+\,\Psi'_0)^{0.5}}\frac{(h\nu\,-\,\Psi'_0)^2}{h\nu} = C_1\frac{(h\nu\,-\,\Psi'_0)^2}{h\nu} \quad \text{for } h\nu \ll E_F \text{ (4)}$$

because the absorptance A is relatively wavelength-independent in the long wavelength region as shown in Fig. 2, the wavelength-independent emission coefficient, C_1, is given by

$$C_1 = \frac{A}{8\,E_F{}^{0.5}\,(E_F\,+\,\Psi'_0)^{0.5}} \quad (5)$$

Figure 5 shows the plots of $\sqrt{\eta}$ hv versus hv for the $Si_{0.7}Ge_{0.3}$/Si HIP and stacked HIP detectors in Fig. 4. As predicted, for $h\nu \ll E_F$ (~ 0.15 eV), the plots are linear, and both the optical potential barriers, Ψ'_0, and the emission coefficients, C_1, can be determined from the plots. Optical potential barriers of 0.054, 0.056, and 0.055 eV, corresponding to cutoff wavelengths of 23.0, 22.1, and 22.5 pm, were determined for the 10- and 30-nm-thick HIP detectors and the stacked HIP detector, respectively. In contrast to the reported 0.020 to 0.05 eV potential barrier discrepancy observed for conventional PtSi detectors [7], similar optical and thermal potential barriers were observed for the $Si_{0.7}Ge_{0.3}$/Si HIP and the stacked HIP detectors, suggesting that the photo-excited holes suffer less inelastic scattering in the $Si_{0.7}Ge_{0.3}$ layers,

The emission coefficients can be used as a figure-of-merit to compare the HIP detectors with different cutoff wavelength. The C_1 determined by the plots were 0.4, 0.19, and 1.38 eV^{-1} for the 10- and 30-nm-thick HIP detectors and the stacked HIP detector, respectively. As expected, C_1 for the 10-rim-thick HIP detector is larger than that for the 30-nm-thick HIP detector, indicating that for the increase of the internal photoemission efficiency due to the reduced $Si_{0.7}Ge_{0.3}$ thickness surpasses the decrease of infrared absorptance. The detector response can be further optimized by reducing the $Si_{0.7}Ge_{0.3}$ thickness. Compared to the 10-rim-thick HIP detector, the two 5-rim-thick p^+-$Si_{0.7}Ge_{0.3}$/30 -rim-thick i-Si multilayers of the stacked HIP detector allowed an efficient internal photoemission due to the reduced $Si_{0.7}Ge_{0.3}$ thickness without any loss of IR absorption. Consequently, C_1 for the stacked HIP detector was ~ 3.5 times that for the 10-rim-thick HIP detector. The higher C_1 of the stacked HIP detector provided a higher response near the cutoff wavelength, as shown in Fig. 4, thereby minimizing the extension of the cutoff wavelength and associated cooling requirements compared to the single-layer HIP detector.

4. SUMMARY

Single-layer and multi-layer $Si_{0.7}Ge_{0.3}/Si$ HIP detectors with cutoff wavelengths out to ~23 µm have been demonstrated. Near-ideal thermionic emission dark current characteristics and photoresponse at wavelength up to 20 µm were measured. Similar optical and thermal potential barriers were obtained, indicating that the HIP is an efficient detector and is suitable for LWIR detection. The use of $Si_{0.7}Ge_{0.3}/Si$ multi-layer of the stacked HIP detector resulted in a significantly increased emission coefficient, C_1, compared to the single-layer HIP detector due to an enhanced internal photoemission efficiency without the loss of IR absorption.

ACKNOWLEDGMENTS

REFERENCES

1. D. J. Sauer, F. V. Shallcross, F. L. Hsueh, G. M. Meray, P. A, Levine, H. R. Gilmartin, T. S, Villani, B. J. Esposito, and J. R. Tower, Proc. SPIE, Vol. 1540, *Infrared Technology XVIII,* edited by B. F. Andresen, M. Scholl, and 1. J. Spiro, pp. 285-296 (SPIE, Bellingham, 1991).

2. J. L. Gates, W. G, Connelly, T. D. Franklin, R. E. Mills, F. W. Price, and T. Y. Wittwer, Proc. SPIE, Vol. 1540, *Infrared Technology XVIII,* edited by B. F. Andresen, M. Scholl, and 1. J. Spiro, pp. 297-302 (SPIE, Bellingham, 1991).

3. D. L. Clark, J. R. Berry, G. L. Compagna, M. A, Cosgrove, G. G. Furman, J. R, Heydweiller, H. Honickman, R. A. Rehberg, P. H. Solie, and E. T. Nelson, Proc. SPIE, Vol. 1540, *Infrared Technology XVIII,* edited by B. F. Andresen, M. Scholl, and 1. J. Spiro, pp. 303-311, (SPIE, Bellingham, 1991).

4. M. Kimata, N. Yutani, and S. N. Tsubouchi, Proc. SPIE. Vol. 1762, *Infrared Technology XVIII,* edited by B. F. Andresen and F. D. Shepererd, pp. 350-360 (SPIE, Bellingham, 1992).

5. P. W. Pellegrini, A. Golubovic, C, E, Ludington, and M. M. Weeks, pp. 157-159, IEEE Tech. Dig. of International Electron Device Meeting (1982)

6. B-Y. Tsaur, M. J. McNutt, R. A. Bredthauer, and R. B. Mattson, IEEE Electron Device Lett., vol 10, pp. 361-363 (1989)

7. T. L. Lin, J. S. Park, T. George, E. W. Jones, R. W. Fathauer, and J. Maserjian, Appl. Phys. Lett., 1993.

8. V. L. Dalal, J. Appl. Phys., 42, 2274 (1971)

9. F. D. Shepherd, Proc. SPIE, Vol. 1735, *Infrared Detectors: State of the Art,* edited by W. H. Makky, pp. 250-261 (SPIE, Bellingham, 1992).

10, T. L. Lin, T. George, E. W. Jones, and A. Ksendzov, Appl. Phys. Lett., vol. 60,380 (1992)

11. T. L. Lin, J. S. Park, S. D. Gunapala, E. W. Jones, and H. M. Del Castillo, submitted to IEEE Electron Dev. Lett.

12. B-Y. Tsaur, C. K. Chen, and S. A. Marine, IEEE Electron Dev. Lett., vol. 12, 293, (1991)

13. F. D. Shepherd, Jr., V. E. Vickers, and A. C. Yang, United States Patent 3,603,847 (1971)

14. J. S. Park, T. L. Lin, E. W. Jones, H. M. Del Castillo, T. Geroge, and S. D. Gunapal, "Long-Wavelength Stacked SiGe/Si Heterojunction Internal Photoemission Infrared Detectors," presented at the 1993 SPIE, San Diego, July, 1993

15. J. I. Pankove, Optical Processes in Semiconductors, (Dover Publishers, New York, 1975), p. 67.

FIGURE CAPTIONS
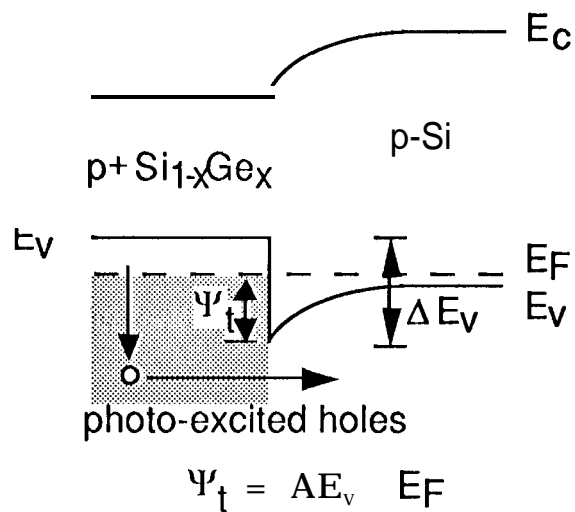
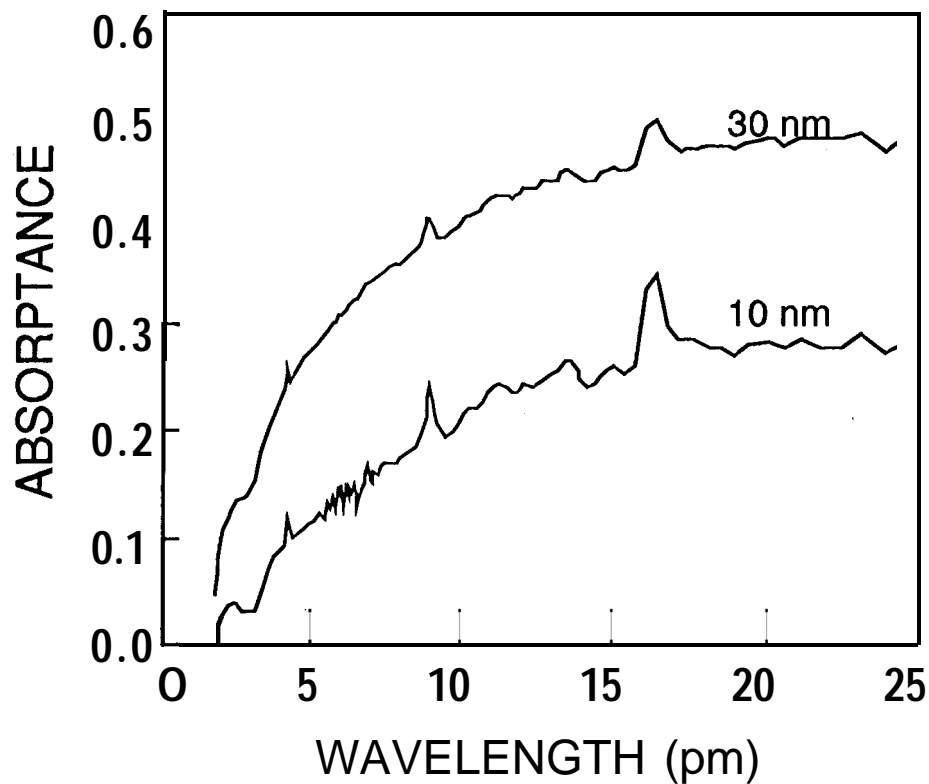Figure 1.   The energy band diagram of the $Si_{1-x}Ge_x/Si$ HIP detector.

Figure 2.   Absorptance measured by FTIR of the 10- and 30-nm-thick $Si_{0.7}Ge_{0.3}$
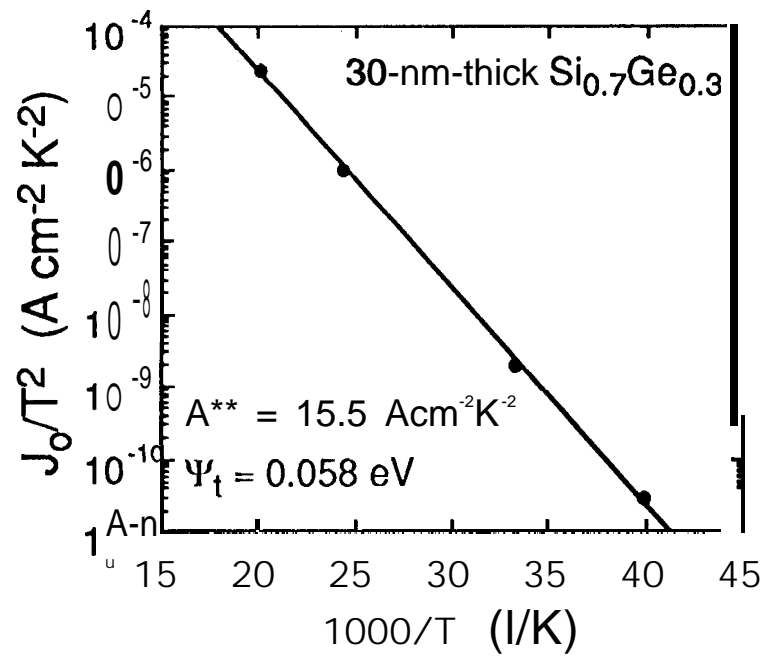   layers grown on p-Si substrates.

Figure 3.   Plot of J_o/T^2 versus 1000/T for the 30-nm-thick $Si_{0.7}Ge_{0.3}/Si$ HIP
              detectors at a reverse bias of 0.5 V.

Figure 4.   Quantum efficiency of the 10- and 30-nm-thick single-layer $Si_{0.7}Ge_{0.3}/Si$
              HIP detectors and the multi-layer stacked HIP detector.

Figure 5.   Plots of $\sqrt{\eta}$ hv versus hv for (a) 10-rim-thick $Si_{0.7}Ge_{0.3}/Si$ HIP detector,
              (b) 30-nm-thick $Si_{0.7}Ge_{0.3}/Si$ HIP detector, and (c) the stacked HIP
              detector with two 5-rim-thick p^+-$Si_{0.7}Ge_{0.3}$/30-nm-thick i-Si multilayers.
              The optical potential barriers, Ψ_0, and the emission coefficients, C_1,
              were determined from the intercepts and the slopes of the linear portions
              of the plots, respectively.

11

TABLE I. Thermal and optical potential barriers, cutoff wavelengths, and emission coefficients of the 10- and 30-nm-thick $Si_{0.7}Ge_{0.3}$/Si single-layer HIP detectors and the stacked HIP detector with two 5-rim-thick p^+-$Si_{0.7}Ge_{0.3}$/30-nm-thick i-Si multilayers.

Detector	10-nm-thick HIP	30-nm-nm-thick HIP	Stacked HIP
Ψ_t (eV)	0.05	0.058	0.053
Ψ_0 (eV)	0.054	0.056	0.055
λ_c (μm)	23.0	22,1	22,5
C_1 (eV^{-1})	0.4	0.19	1.38

Figure 1,   The energy band diagram of the Si·$_{-x}$Ge$_x$/Si HIP detector,

Figure 2.   Absorptance measured by FTIR of the 10- and 30-nm-thick Si$_{0.7}$Ge$_{0.3}$
                 layers grown on p Si substrates.

Figure 3.   Plot of J_0/T^2 versus 1000/T for the 30-nm-thick $Si_{0.7}Ge_{0.3}/Si$ HIP detectors at a reverse bias of 0.5 V.
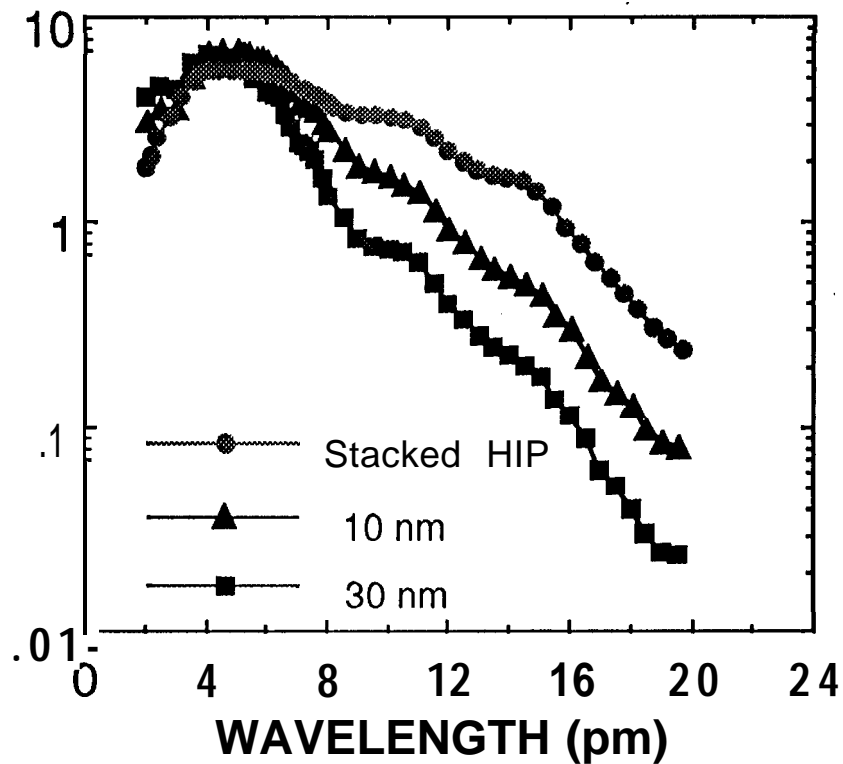

Figure 4.   Quantum efficiency of the 10- and 30-nm-thick single-layer $Si_{0.7}Ge_{0.3}/Si$ HIP detectors and the multi-layer stacked HIP detector.

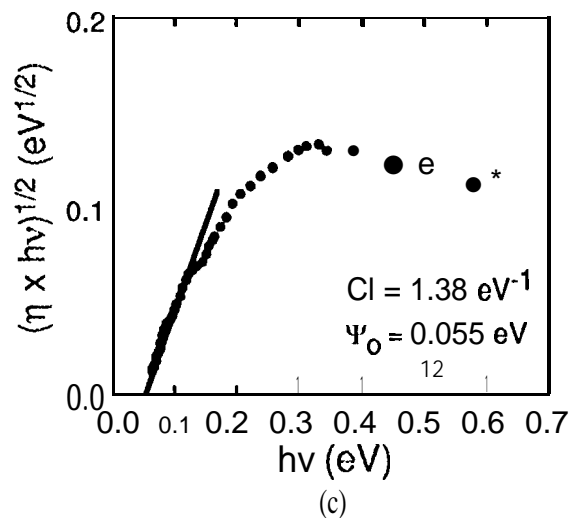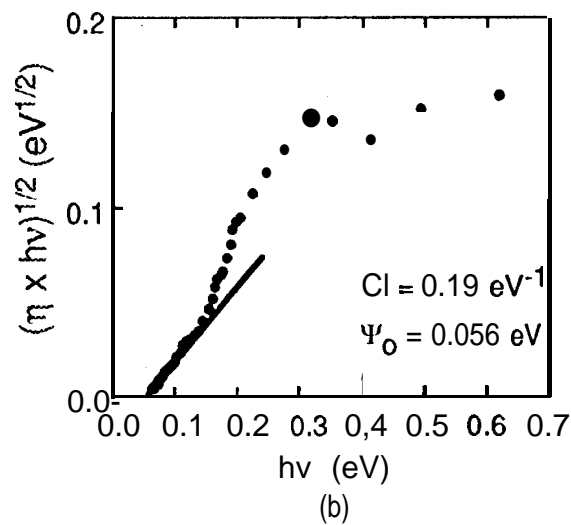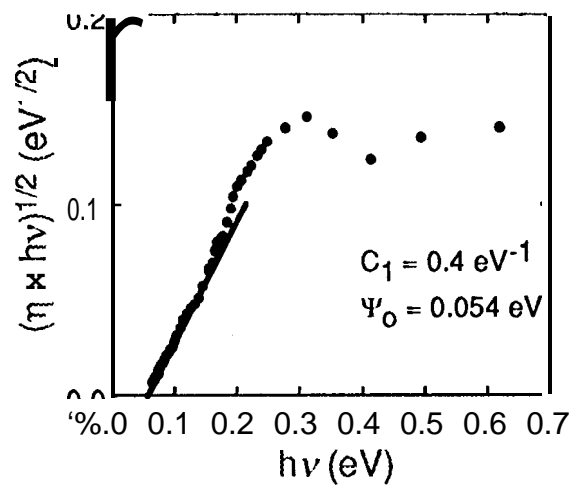Figure 5.   Plots of $\sqrt{\eta \, h\nu}$ versus hv for (a) 10-rim-thick $Si_{0.7}Ge_{0.3}/Si$ HIP detector, (b) 30-nm-thick $Si_{0.7}Ge_{0.3}/Si$ HIP detector, and the stacked HIP detector with two 5-rim-thick $p^+-Si_{0.7}Ge_{0.3}/30$-nm-thick i-Si multilayers. The optical potential barriers, Y'_o, and the emission coefficients, C_1, were determined from the intercepts and the slopes of the linear portions of the plots, respectively,